On the use of a mesoscale masonry pattern representation in discrete macro-element approach

Federica Vadalà[1], Valeria Cusmano[2], Marco Francesco Funari[1,*], Ivo Caliò[2] and Paulo B. Lourenço[1]

[1]Department of Civil Engineering, University of Minho, ISISE, 4800-058 Guimarães, Portugal

[2] Department of Civil Engineering and Architecture (DICAR), University of Catania, Italy.

[*]Correspondence: marcofrancesco.funari@civil.uminho.pt

Abstract

This paper presents numerical investigations using the mesoscale approach coupled with the discrete macro-element approach for masonry structures, i.e., each macro-element represents a single unit stone. At first, parametric analyses are performed on a U-shape masonry prototype made with stone. Nonlinear static analyses are performed to investigate parameters that affect the results when a mesoscale masonry pattern representation is adopted. Results demonstrate how mesoscale representation is a powerful alternative to model unreinforced masonry structures within a discrete macro-element approach (particularly if compared with classic homogeneous FE methodologies). However, one of the main challenges in using the mesoscale approach for the structural assessment of masonry buildings, made with stones having different dimensions, is the unit by unit description. The complexity of the problem, and the amount of information needed, usually preclude the study of these structures deterministically. To this end, a digital tool to generate randomised masonry patterns using a few input parameters is proposed. A box structure is adopted as parent geometry, and ten masonry patterns with different degrees of randomness are investigated by performing nonlinear static and dynamic simulations. The outcomes focus on the influence of masonry patterns and demonstrate how irregularity of units can affect the structural response leading to a reduction in terms of strength and ductility if compared to regular distribution of masonry units.

Keywords: Unreinforced masonry structures; Mesoscale approach; non-periodic masonry pattern; DMEM.

1 Introduction

Field reconnaissance after earthquake events demonstrated how out-of-plane (OOP) failure mechanisms affect historical unreinforced masonry (URM) structures, producing their collapse, loss of life, and, at the same time, an immaterial loss of memory and people identity [1]–[3]. As a consequence, in the last decades, several researchers proposed advanced analysis methods, often calibrated through extensive experimental campaigns [4]–[9], for the preventive assessment of heritage buildings. Their overall classification is mainly made between numerical and analytical approaches [10], [11].

Analytical approaches are often based on limit analysis theorems that have the great advantage of being independent of most material properties but inevitably rely on a very simplified material model [12]–[15]. Such approaches include force- and displacement-based procedures suitable for rapid seismic vulnerability assessment. Moreover, limit analysis-based tools typically neglect the structure's global behaviour, only focusing on assessing a set of local failure mechanisms [16]–[20].

Numerical approaches are typically implemented in the Finite Element Method (FEM) [21]–[27] or Discrete Element Method (DEM) [28]–[32] frameworks. Such approaches model the masonry material using different representation scales, i.e., equivalent continuum, macro-blocks, or discrete representations. FEM allows a more versatile application as masonry can be represented either through a homogeneous equivalent media (designated macro-modelling) or by a discrete representation of units and joints (designated micro-modelling). DEM is well suited for masonries with both dry- and mortared joints but still requires a full representation of the blocks (masonry units) arrangement [32]–[37]. In both cases, linear and nonlinear static and dynamic analyses are eligible.

Nonetheless, additionally, to the significant amount of data needed to characterise the nonlinear response of materials, the analysis can be both time-consuming and computationally expensive when estimating the ultimate ductility level of the structure. Despite their reliability, the computational efficiency of the available numerical methods is rarely compatible with the need to have a rigorous real-time post-earthquake assessment [38]. Hence, several research groups developed alternative modelling approaches and practical tools to decrease the computational cost of nonlinear static and dynamic analyses [39]–[42].

In this framework, macro-element approaches were proposed in which structures are described as an assemblage of macroscopic structural elements. For instance, the Equivalent Frame Model (EFM) is being adopted by national and international standards in combination with nonlinear static analysis [43]. Because of its simplicity and low computational demand, it is one of the most widely adopted analysis methods in engineering practice [44]. However, despite the advantages of the EFM method, it is worth underlining some limitations: i) discretisation of structure with an irregular position of openings is sometimes ambiguous or not possible, ii) geometric inconsistency of the approach, as it represents a plane portion such as masonry panels with a mono-dimensional element, iii) presence of areas which cannot be damaged, generally identified as rigid links, iv) the ultimate displacement is a priori defined. In order to cover such limitations and keep the computational efficiency, a discrete macro-element method (DMEM) was proposed in Ref. [45]. The first implementation of the DMEM approach was based on a plane element whose kinematics was described only by four Lagrangian parameters: three degrees of freedom associated with the in-plane (IP) rigid-body motion and one additional degree of freedom related to shear deformability in its own plane. Such plane elements were represented by articulated quadrilaterals with rigid edges connected to the vertices by four hinges and diagonal springs simulating the shear behaviour. Each element was connected to the adjacent ones by means of a discrete distribution of nonlinear springs, denoted as interfaces. The interfaces' deformations are associated with the relative motion of the connected panels, and no additional Lagrangian parameters are needed. One can note how this preliminary formulation of the DMEM approach simulated the nonlinear behaviour of masonry panels IP, not being able to describe the out-of-plane (OOP) behaviour. The reliability of the proposed approach was evaluated by means of nonlinear incremental static analysis performed on masonry structures, for which theoretical and/or experimental results are available in the literature [45]. Afterwards, the macro-element was improved to investigate OOP response of URM structure by developing a three-dimensional macro-element for which its kinematic was described by seven degrees of freedom IP and OOP [46]. Subsequently, such an element was adopted to simulate also curved masonry structures, whose role is fundamental both in the local and global behaviour of the buildings, especially in the monumental ones (e.g. arches, vaults, and domes) [47]. Both experimental and numerical validations showed the capability of the proposed approach to be applied to predict the nonlinear response of URM structures under different loading conditions. A more recent implementation was conducted to assess the seismic behaviour of URM structures subjected to dynamic input, i.e., earthquakes records, by introducing a consistent or lumped mass matrix [48]. As demonstrated in Ref. [48], the DMEM strategy showed its capability to simulate dynamic response characterised by coupling IP/OOP failure mechanisms. Despite the improvements recently implemented in the DMEM approach, some limitations still characterised such a methodology, i.e., i) formulation accounts only for small displacements, ii) macro elements size dependency when the structure is affected by OOP loading, iii) vertical joints do not permit to account for interlocking phenomenon typically expected in masonry structures. However, the literature analysis underlines how the DMEM approach may be used to assess the seismic behaviour of historic masonry structures. Nevertheless, just a few attempts investigated the influence of the mesh discretisation of the macro-elements, how the same impacts the structural response, and the potential in adopting a mesoscale representation [49]. In order to address these gaps, this paper mainly aims to: i) apply the DMEM approach by adopting a mesh representation consistent with real masonry patterns and ii) evaluate what phenomenon affects the structural response. To accomplish the latter, the framework described next has been followed:

1. The 3D macro-element is adopted to simulate the OOP response of masonry structures.
2. Parametric investigations are performed on U-shape masonry prototypes made with stone [50]. Modelling parameters are investigated and discussed, and the motivation in using mesoscale mesh discretisation is underlined.
3. A random mesh generator is implemented to quickly generate numerical models where the masonry patterns are consistent with a chaotic distribution of the units.
4. The random mesh generator tool is used to generate ten different masonry patterns consistent with a unique parent geometry. The masonry prototypes differ only in terms of masonry patterns and openings.

The novelties of the study include: i) a pioneering application of the mesoscale random generated masonry pattern representation in DMEM for simulating unreinforced masonry structures, ii) numerical investigation of the phenomenon that affects the structural response when mesoscale representation is adopted, and iii) implementation of a visual script for the generation of different masonry wall patterns. The paper is organised as follows. Section 2 summarises the theoretical formulation and the numerical implementation of the DMEM approach. Section 3 presents a parametric study to assess how the mesh topology affects the structural response and reports comparisons between classical DMEM and finite element homogenous approaches. Section 4 investigates how different degrees of randomness affects the seismic behaviour of a benchmark case. Finally, conclusions are discussed in Section 5.

2 Discrete Macro-Element Modelling Approach

As mentioned in the previous section, the original formulation of the DMEM approach provided only the possibility to simulate the IP structural response of masonry panels, which were modelled using a simple plane element (Figure 1a). In order to overcome this issue, a macro-element that was able to simulate the OOP response was proposed in Ref. [47]. Such a macro-element is a zero-thickness element, which is able to account for shear deformation in its plane, having on the edges a set of different nonlinear links denoted as interfaces. Each interface is constituted by i) m rows of n orthogonal nonlinear links, responsible for simulating the panels' flexural behaviour (Figure 1b and Figure 1c), ii) a single IP sliding link, which rules for the sliding behaviour, and iii) a set of two OOP sliding links that account for both OOP sliding and torsional behaviour. One can note that the number of orthogonal links is selected in accordance with the desired level of accuracy, losing as a counterpart a little computational efficiency. The diagonal shear deformability is governed by a diagonal nonlinear link that connects two corners of the quad element [46]. Hence, the kinematics of the spatial macro-element are described by seven Lagrangian parameters, six governing the rigid body motion and the remaining associated with the IP shear deformability. One can note that the low number of DOFs associated with each macro-element makes this approach computationally inexpensive with respect to the classical FEM and DEM formulations.

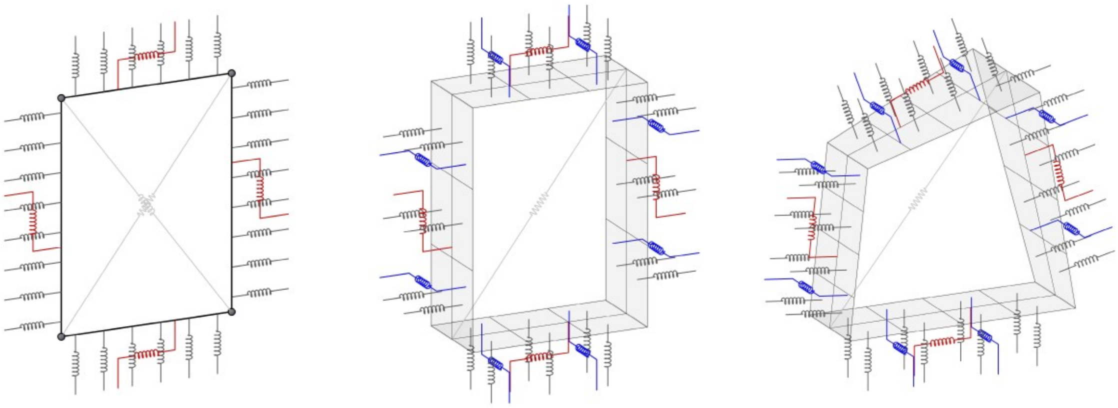

(a) (b) (c)

Figure 1: DMEM evolution (a) Plane Element; (b) Regular Spatial Element; (c) Irregular Spatial Element.

Macro-element's nonlinear links calibration has been performed according to a straightforward fibre calibration procedure. The procedure reported herein is suitable for three-dimensional model characterised by elements with the same geometrical and mechanical characteristics. Nevertheless, the calibration procedure of nonlinear links associated with irregular three-dimensional panels characterized by different mechanical properties presents a more sophisticated procedure beyond this research's scope. A detailed description of the calibration procedure for irregular macro-elements, can be found in Ref. [51]. The nonlinear interface's links can be distinguished as transversal N-links, IP shear sliding N-link, and OOP shear sliding N-links. In the following, the main characteristics of the calibration procedure are described with reference to each group of nonlinear N-links.

Transversal N-links orthogonal to the interfaces govern the flexural IP and OOP behaviour between two adjacent macro-elements. Each orthogonal link is representative of the nonlinear behaviour of the corresponding masonry strip of two adjacent elements (e.g. panels l and k) along a given material direction. Since the deformations of the panels are concentrated in the zero-thickness interfaces, the orthogonal links have the role of simulating the deformability of the two connected panels in a given direction. It is worth noting that to account for masonry as an orthotropic material, the calibration is conducted separately for horizontal and vertical interface elements. The initial stiffness K_n of each link is simply obtained by assigning, to each link, the axial rigidity (Young's modulus, E) of the corresponding masonry strip defined by the volume characterised by the influence area (A_{Sn}) of each spring and half of the length ($L/2$) of the panel (Figure 2a). This procedure provides a couple of springs in series, each associated with each of the connected panels. Each couple of springs is then replaced by a single resulting nonlinear spring as described in [45]. The yielding forces in tension, F_{ytn}, and compression, F_{ycn}, of each transversal link are related to their influence area and the tensile, σ_t, and compressive strengths, σ_c, adopted for the masonry. Finally, the tensile and compressive yieldind displacements u_{ytn} and u_{ycn} are associated with each link's yielding forces and initial stiffness. The nonlinear behaviour of the masonry can be simulated by adopting for transversal links any suitable and uniaxial nonlinear constitutive laws. Initial stiffness, tensile and compressive strength and displacement are reported respectively in Eq. 1-5.

$$K_n = 2\frac{EA_{Sn}}{L} \tag{1}$$

$$F_{ytn} = A_{Sn}\sigma_t \tag{2}$$

$$F_{ycn} = A_{Sn}\sigma_c \tag{3}$$

$$u_{ytn} = \frac{F_{ytn}}{K_n} \tag{4}$$

$$u_{ycn} = \frac{F_{ycn}}{K_n} \tag{5}$$

The shear deformation of a masonry wall, discretised by a mesh of macro-elements, can be partly related to the diagonal shear deformation and partly due to the friction sliding along the interface between two adjacent macro-elements. The former is governed by a single diagonal spring (Figure 1) connecting two opposite macro-elements vertexes. First, a linear elastic calibration is performed by enforcing the equivalence between the macro-element subjected to a pure shear deformation related to the kinematic of the hinged quadrilateral and a reference continuous elastic solid. This finite portion of masonry is characterised by shear modulus G, transversal area A_t, height h, and base b. The initial stiffness K_D of the diagonal link is expressed in Equation 6, in which θ is defined as arctan(b/h), and it is influenced by a shear factor denoted as α_s whose value ranges between 0 and 1. If this factor presents a value equal to 1, the global in-plane shear stiffness is entirely associated with the initial stiffness of the diagonal links, and the in-plane sliding links are assumed rigid. On the other hand, if the value of α is different from 1, the global in-plane shear stiffness comes as a contribution between diagonal and in-plane sliding nonlinear links.

$$K_D = \frac{G \cdot A_t}{h \cdot cos^2\theta \cdot \alpha_s} \quad (6)$$

The nonlinear post-elastic behaviour may be addressed by adopting different and suitable constitutive laws. A Mohr-Coulomb or Turnsek-Cacovic yielding criteria can be adopted for the constitutive calibration of this nonlinear link. The value of yielding force F_y associated to the Mohr-Coulomb and Turnsek and Cacovic [52] criteria are given by Equations 7 and 8, respectively.

$$F_y = F_{y0} + \mu_d \cdot N \quad (7)$$

$$F_y = F_{v0}\sqrt{1 + \frac{N}{1.5 \cdot F_{v0}}} \quad (8)$$

where F_{y0} and F_{v0} are the yielding forces under no confinement conditions (zero normal stresses) associated with the Mohr-Coulomb or Turnesek-Cacovic criteria.

The IP and OOP shear sliding springs (Figure 2b) rule the relative sliding motion between two adjacent macro-elements. The initial stiffness K_S, related to the sliding mechanism, is associated with the panel's shear modulus G, the effective length, and the influence area A_s of the corresponding nonlinear link. The expression that provides the initial stiffness for IP and OOP sliding links is given by Equation 9. It is worth mentioning that the OOP shear mechanism is solely associated with the nonlinear links along the thickness of the interface element, and there is no need to introduce a shear factor in the out-of-plane direction. The OOP sliding links also account for torsional behaviour around the axis orthogonal to the interface plane (Figure 2c). The elastic torsional stiffness K_ϕ is associated with a torsional rigidity factor J_ϕ given by Equation 11, in which s corresponds to the thickness of the panel. The shear sliding behaviour of UMR structure is associated with a frictional phenomenon along the mortar joints. Such behaviour can be adequately simulated by means of a Mohr-Coulomb yielding criterion. Based on this approach, the current yielding force F_y of the IP and OOP links is defined employing the cohesion c and friction coefficient μ_s of the masonry material, the current contact area A, and the normal force N applied to the interface element.

$$K_S = \frac{G \cdot A_s}{L \cdot (1 - \alpha_s)} \quad (9)$$

$$K_{\Phi} = \frac{G \cdot J_{\phi}}{L} \tag{10}$$

$$J_{\phi} = \mathrm{B} \cdot s^{3}\left[\frac{1}{3} - 0.21\frac{s}{B}\left(1 - \frac{s^{4}}{12 \cdot B^{4}}\right)\right] \tag{11}$$

$$F_{y} = c \cdot A + \mu_{s} \cdot N \tag{12}$$

More details on the calibration procedures can be found in Refs. [45], [46]. One can note that different nonlinear constitutive laws for the shear mechanisms accounting for residual strength when a target displacement is attained might be adopted. However, it has not been considered in the present paper since the main goal of this study relies on the investigation of the masonry mesoscale masonry pattern representation in a DMEM approach. For this reason, simple constitutive laws have been adopted aiming at limiting the number of parameters involved in the numerical analyses.

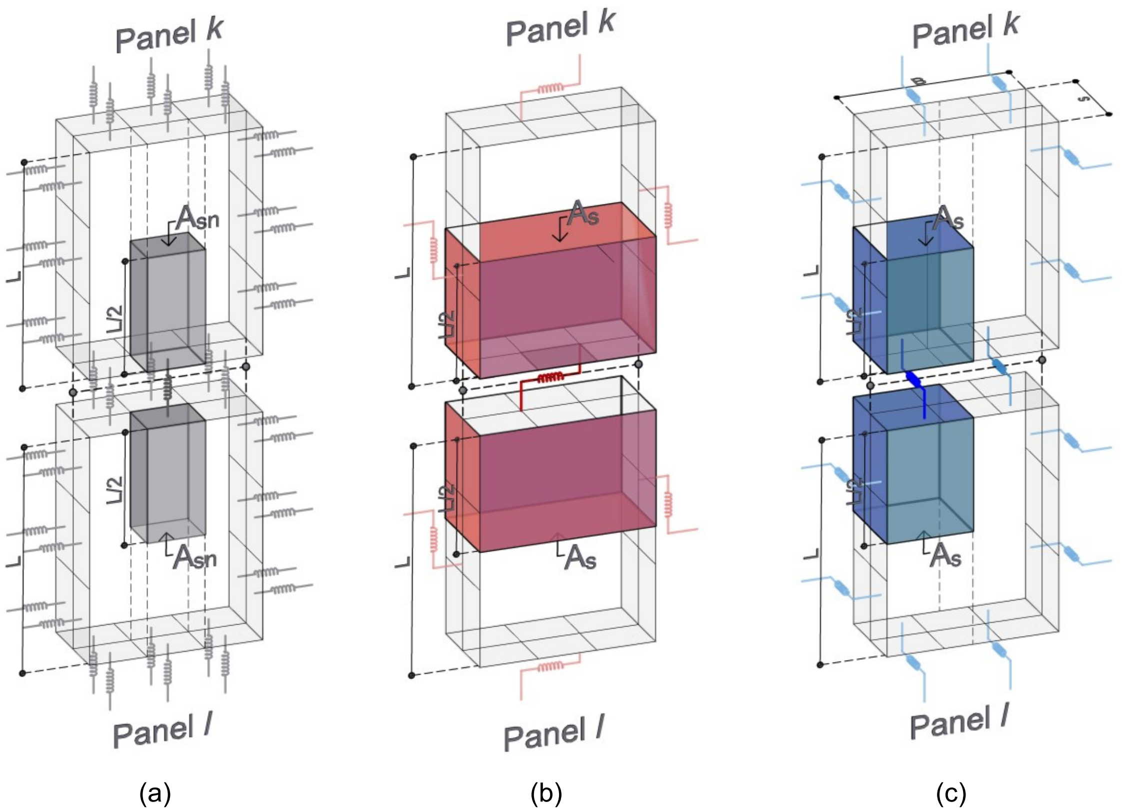

Figure 2: Interface’s Links representation: (a) Orthogonal N-Links; (b) In-plane sliding N-links; (c) Out-of-Plane sliding N-Links.

DMEM approach classical interpretation implies that each macro-element must be representative of the corresponding finite portion of masonry walls, according to the macro-modelling approach.

Consequently, there is no relation between masonry constituents and block regions, and a homogenisation strategy is adopted to define the masonry mechanical constitutive law.

An example of a masonry wall is shown in Figure 3a. Even though DMEM is conceived as a macro-modelling strategy, some studies (Figure 3b) explored the possibility of discretising the structural model within a mesoscale approach (Figure 3c) [49], [53]. In this case, the properties of the constituents, for example, brick and mortar, and the details of the masonry arrangement are adopted to study the interaction of the constituents and the damage propagation pattern under different loading histories. It is worth noting that by using mesoscale strategies, some physical phenomena involved can be described in more detail, i.e. interlocking effect between the blocks or the presence of well-defined and realistic fracture surfaces at the interface. Moreover, a mesoscale model is quite accurate for the study of weak or dry mortar masonry structures for which usually DEM approaches are adopted [28], [29], [54]. Therefore, depending on whether a macro- or mesoscale approach is adopted, it is necessary to appropriately calibrate the main mechanical parameters that influence the response. As reported in Ref. [49], the interlocking phenomenon has mainly the effects of increasing the tensile strength and the cohesion between blocks influencing the collapse mechanism and increasing the strength and displacement capacity of the entire structure.

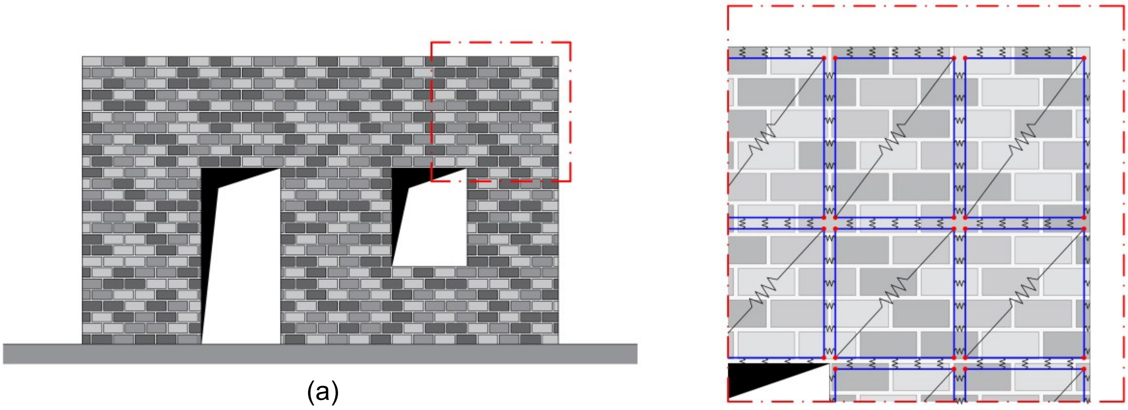

(a) (b)

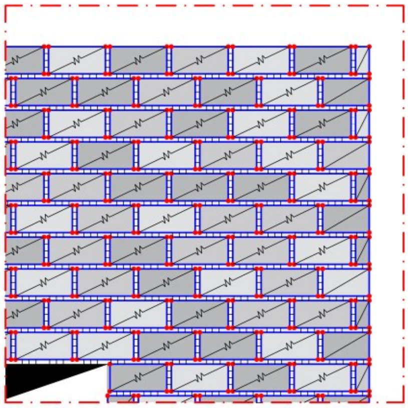

Figure 3: (a) Real blocks' arrangement; (b) Macro-scale modelling; (c) Mesoscale modelling.

3 Numerical Investigation: U-shape Stone Prototype

3.1 Description of the prototype

In this section, parametric studies are performed to assess how the mesh topology affects numerical simulations performed with the DMEM. The numerical investigation has been performed on a benchmark represented by a U-shape masonry prototype, a simple structure of three walls forming a U-plan made in stone masonry that idealises the experimental tests performed at the LNEC shaking table [55]. Figure 4 represents the overall geometrical characteristic of the masonry prototype.

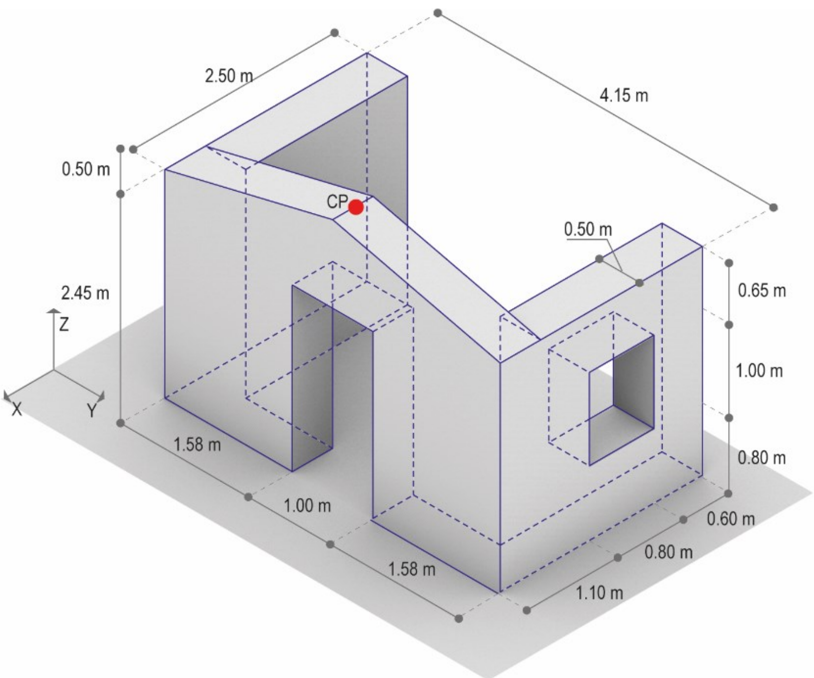

Figure 4: U-Shape stone prototype: geometrical features.

Figure 5 represents the different mesh discretisations adopted. Three of them are mesh discretisations consistent with the macroscale approach, in which the macro-elements' characteristic dimension is gradually decreased to reach three different levels of refinement. The last one is a mesoscale discretisation, which is taken in agreement with the one adopted in Ref. [56]. Concerning the mechanical properties, the parameters reported in Ref. [56] have been initially adopted for all mesh discretisations (Table 1 and Table 2). It is worth underlining that when a mesoscale representation is adopted (M4), a linear-elastic constitutive law has been selected for the diagonal shear behaviour to avoid that diagonal cracking involves the single macro element. This assumption ensures that the shear failure does not occur when macro-element represents a single masonry unit [49].

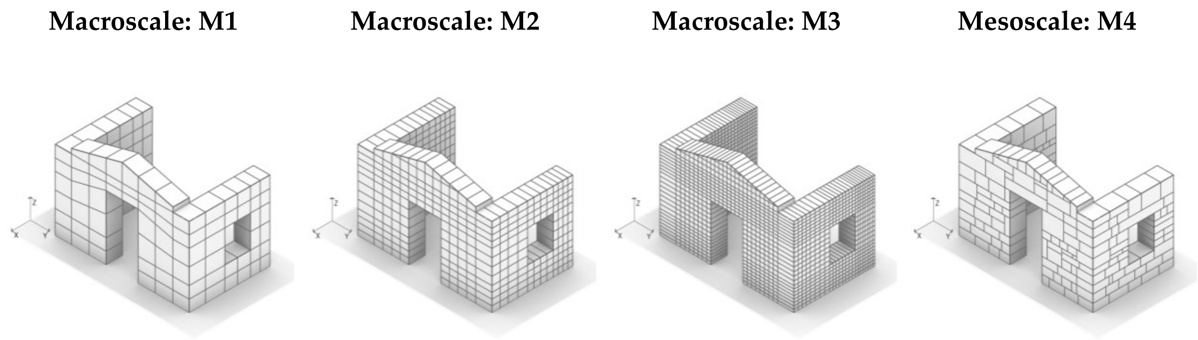

Figure 5: Mesh discretisations adopted for the numerical investigations.

Table 1: Mechanical properties adopted for the U-shape prototype: flexural behaviour [56].

	Flexural behaviour					
	Density	**Young's modulus**	**Compressive strength**	**Compressive fracture energy**	**Tensile strength**	**Tensile fracture energy**
Model	**[kg/m^3]**	**[MPa]**	**[MPa]**	**[N/mm]**	**[MPa]**	**[N/mm]**
M1,M2,M3	2360	2077	5.44	∞	0.224	0.048
M4	2360	2077	5.44	∞	0.224	0.048

Table 2: Mechanical properties adopted for the U-shape prototype: shear behaviour [56].

	Diagonal cracking behaviour				Sliding behaviour	
	Shear modulus	**Failure criterion**	**τ_0**	**μ_d**	**c**	**μ_s**
Model	**[MPa]**		**[MPa]**		**[MPa]**	
M1,M2,M3	830	Mohr-Coulomb	0.336	0.3	0.336	0.3
M4	830	-	-	-	0.336	0.3

3.2 Nonlinear static analyses

This section aims to investigate how the structural response o if macro- and mesoscale masonry representations are adopted. Nonlinear static analyses have been performed applying vertical actions including gravity loads and, subsequently, an incremental lateral force along the positive direction of axis X.

Figure 6a reports the load-displacement curves of the considered mesh discretisations for horizontal actions. Further comparison is provided with a homogeneous model performed in Abaqus [57] where concrete damage plasticity (CDP) has been adopted to simulate the nonlinear behaviour of the masonry. The results demonstrate how the M1, M2 and M3 models are slightly affected by a mesh dependency, showing small differences in terms of initial stiffness and peak load. On the contrary, the mesoscale model, i.e., M4, provides a stiffer initial behaviour and a higher peak load than the M1, M2 and M3. One can note how M4 has the same initial stiffness as the homogeneous model performed in Abaqus; however, the reached peak load is slightly higher than the macroscale discretisations, which cannot account for blocks' interlocking. When mesh discretisation with interlocking between blocks are considered, the structural response is characterised by a complex interaction between the macro-elements that involved shear sliding, shear diagonal, torsional, and membrane behaviour.

The mesoscale model M4 correctly accounts for the stone's interlocking effects leading to higher stiffness and ultimate load. Moreover, M1, M2 and M3 present similar post-peak behaviour, while M4 has two drops. Generally, when a discrete numerical model is used, each drop corresponds to a local crack in the numerical model. Once again, the differences in the post-peak behaviour can be justified by the fact that the mesoscale model M4 correctly accounts for the stone's interlocking effects, leading to different and more realistic results in terms of loading-displacement curve and collapse mechanism. In this latter model, the first drop, in the loading-displacement curve, is due to the crack propagation that starts from the opening in the later wall, whereas the second drop is related to the flexural rocking mechanism of the orthogonal wall without openings in its plane, which causes compressive and tensile stresses at the base of the wall. When the tensile stress exceeds the tensile strength assumed for the masonry, cracks propagate at the base of the wall. M4 model grasps the so-called flange effect that can cause a significant overstrength on the approach based on equivalent frame modelling [58].

The misalignment of the vertical interfaces of the model M4 leads to more realistic results also in terms of collapse mechanisms, as reported in Figure 7, where the failure mechanisms provided by the five considered models are compared. To this end, for taking into account the interlocking effects provided by the mesoscales model by using a macroscale simulation, it is needed to consider the over-stiffness and over-strength in the calibration of the mechanical parameters, particularly when the size of the units is large in comparison of the size of the structural components of the building. According to Ref. [31], the tensile strength and fracture energy have been modified to obtain pushover curves comparable to those relative to the mesoscale model. Hence, the updated macroscale model (DMEM-C) has the same mesh discretisation adopted for M1, whereas tensile strength and fracture energy were calibrated through a tuned process, which was stopped when assumed a value equal to 0.240 MPa and 0.060 N/mm, respectively.

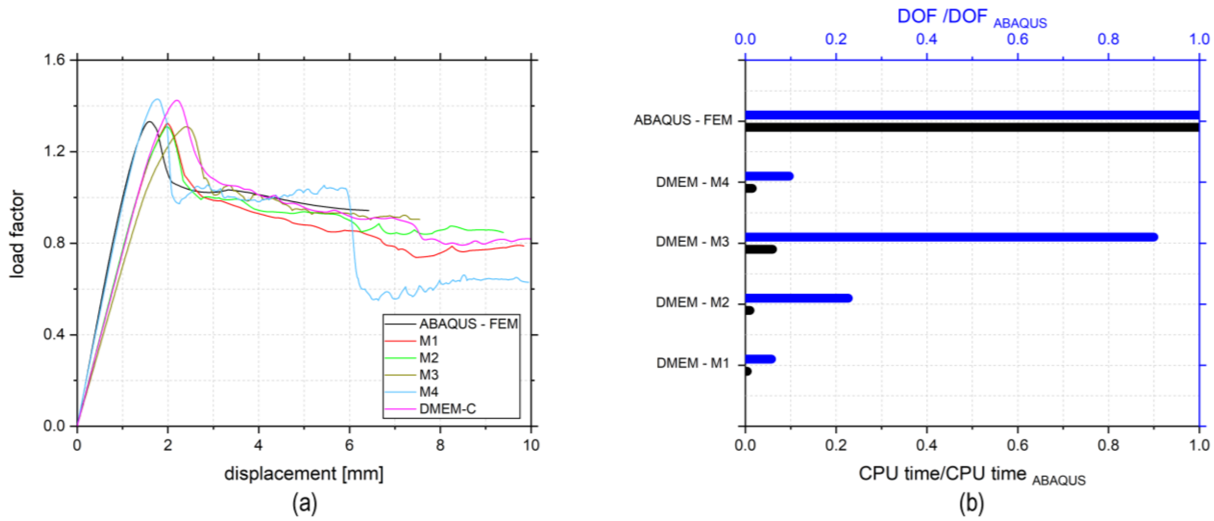

Figure 6: (a) Comparison in terms of load-displacement curve; (b) Normalised computational time (CPU) and normalised number of degrees-of-freedom (DOFs) for each numerical simulation.

One can note how M4 and DMEM-C curves show a different initial stiffness. Such a phenomenon may be mitigated by also modifying the elastic modulus of the masonry in the DMEM-C model. Finally, Figure 6b reports a comparison including the required computational time (CPU) and the number of degrees-of-freedom (DOFs) for each mesh discretisation. Results have been normalised with respect to the Abaqus model. It should be noted how the DMEM approach can strongly decrease the computational demand, by more than 90%. Besides, when a mesoscale mesh representation has been used, the computational saving is more than 95%, while the amount of DOFs is decreased by 90%.

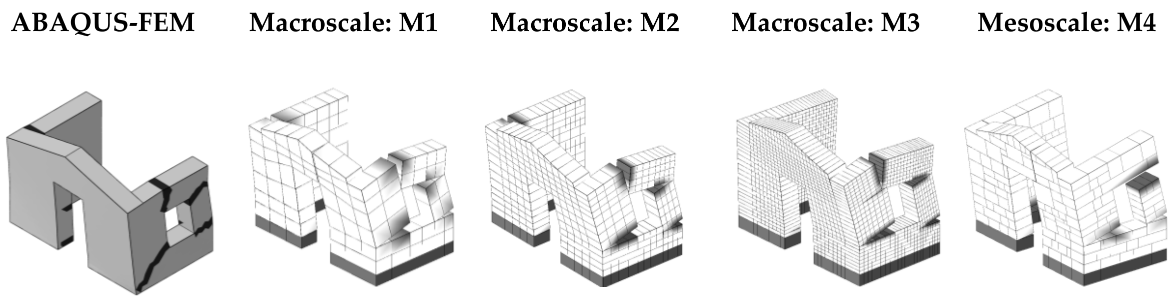

Figure 7: Comparison in terms of failure mechanisms.

In short, the mesoscale representation may be a powerful alternative to model unreinforced masonry structures within a discrete macro-element approach (particularly if compared with classic homogeneous FE methodologies), even though the mechanical calibration cannot be performed considering an equivalent homogenous masonry, as described in the previous section 2. Differently, a proper characterisation of the blocks and the mortar joints must be considered.

4 Numerical Investigation: Box prototype

4.1 Generation of the models: geometrical and mechanical characteristics

As reported in Ref. [59], masonry constituted by the assemblage of blocks and stones with variable dimensions is very common in historical buildings. However, the complexity of the problem, and the amount of information to accurately model using a mesoscale approach, usually preclude the study of these structures deterministically. Indeed, such uncertainties suggest investigations based on probabilistic approaches rather than deterministic, i.e., assuming texture properties within certain statistical variations.

This section is devoted to understanding how irregular masonry patterns affect the structural response of a masonry prototype having a rectangular shape. Several mesh discretisations having a different degree of randomness have been generated by adopting a proper numerical tool which is described below. Instead, the parent geometry is always the same and coherent with a rectangular plan having 4.80 m and 7.20 m, with walls' height equal to 4.0 m and a walls' thickness of 0.30 m (Figure 8). The overload arising from a deformable slab, having a weight equal to 150 kN/m2, has been modelled as distributed line load along the top of the walls W2 (Figure 8).

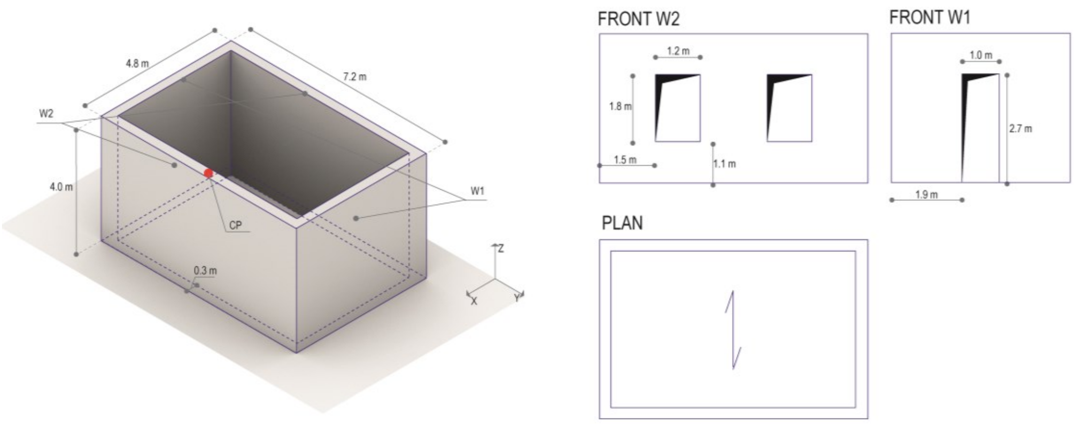

Figure 8: Parent geometry for box prototype: geometrical features.

The masonry patterns have been generated using a numerical tool implemented in a GHPython script [42], [43]. It can generate 2D or 3D masonry prototypes within a randomised masonry pattern. However, one can note that the GHPython script is responsible for generating a single planar wall, whereas the assemblages in 3D still require operations performed that have been manually implemented. Next, the tool's explanation is performed in 2D framework, i.e., referred to the generation of a single planar wall. As represented in Figure 9a, the primary tool's inputs are the overall dimension of the wall (height, length and width), the cantonal's dimension, and the number of units' courses (N_R). At this stage, the user has to define some parameters defining three numerical domains. As reported in Figure 9b the first domain is formed by integer numbers that define the minimum and the maximum number of units per row (U_R). The second domain of values is defined by the smallest and the largest unit length that may appear at each row (U_L). Finally, the third domain, similar to the second one, is defined by the minimum and maximum height that may assume a units' course (U_H) (Figure 9c). Finally, the total height of the wall is scaled in order to be consistent with the primary input of the generator. The proposed algorithm can randomise the values contained inside the early mentioned domains and generate a different masonry pattern at each iteration.

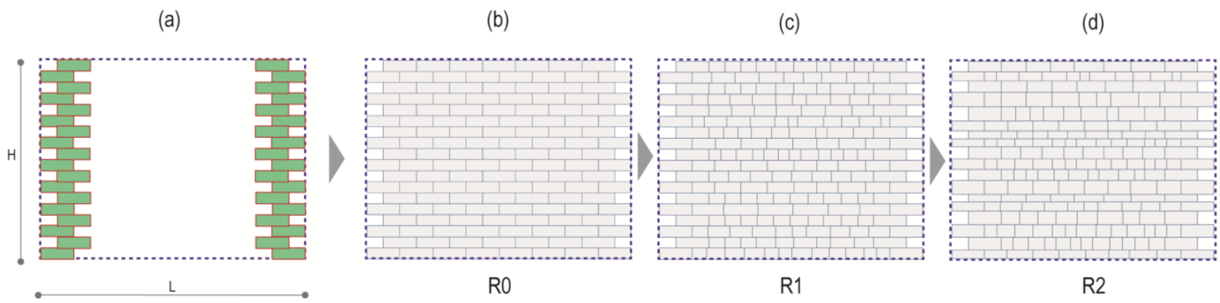

Figure 9: Random masonry pattern generation.

Referring to the parent geometry reported in Figure 8, one can note that two subcategories of masonry patterns have been generated, which are characterised by a different number on the units' courses equal to (A) 18 and (B) 12, respectively. The investigated mesh configurations are reported in Figure 10. A regular masonry bond pattern characterises the reference configurations A1 and B1, where all the units have the same dimensions, i.e., 0.60 x 0.222 x 0.30 m^3 and 0.60 x 0.333 x 0.30 m^3, respectively.

A chaotic mesh distribution instead characterises A2 and B2 configurations. Therefore, the following values for the domains U_R and U_L have been adopted:

$$U_R^{W1} = [6, 10] \tag{13}$$

$$U_R^{W2} = [9, 15] \tag{14}$$

$$U_L^{W1,W2} = [[0.20,0.60], 1.00] \tag{15}$$

where the limits W1 and W2 are referred to walls having smaller and larger lengths (see Figure 9). One can note how $U_L^{W1,W2}$ does not contain the actual dimension of the blocks, but the ratio between a lower bound, which has been assumed to be randomly selected between 0.20 and 0.60, and the upper bound that is equal to 1.00. The value selection is random and is performed by using the random function available in Python [60]. Hence, a remapping procedure must be performed in order to respect the compatibility condition regarding geometry:

$$\sum_{U_R} U_L/(L - L_{cant}) = 1 \tag{16}$$

Finally, A3 and B3 are also affected by a variable height of the units' courses. In this case, the domain U_H has been defined as follow:

$$U_H = [0.50, 1.00] \tag{17}$$

One can note that U_H does not contain the actual height of the unit's course, but the ratio between a lower bound, assumed to be 0.50, and the upper bound that is equal to 1.00. Hence, a remapping procedure must be again performed in order to respect the following compatibility condition:

$$\sum_{N_R} U_H/(H) = 1 \tag{18}$$

Finally, the openings are added by making Boolean differences and introducing the lintels.

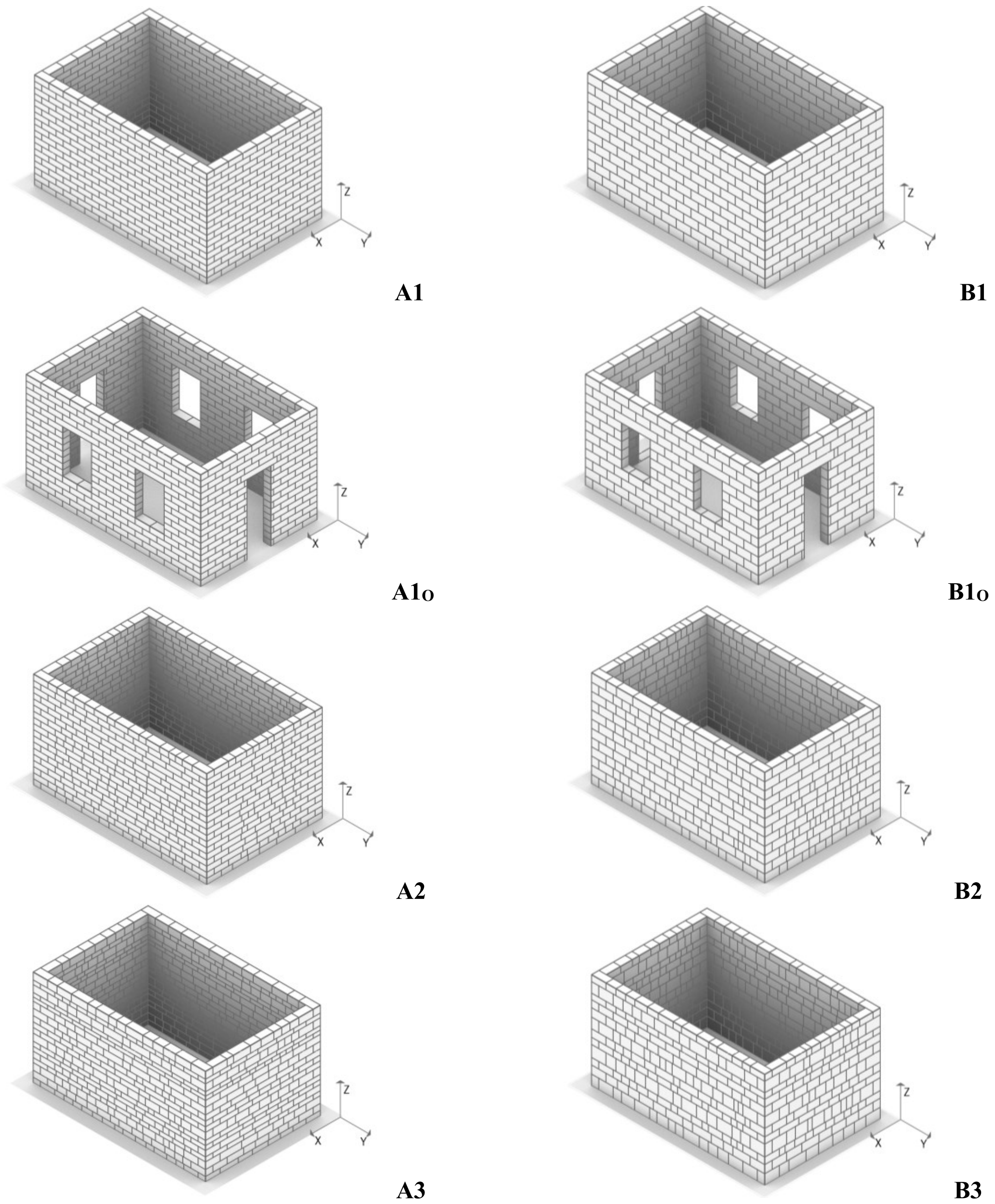

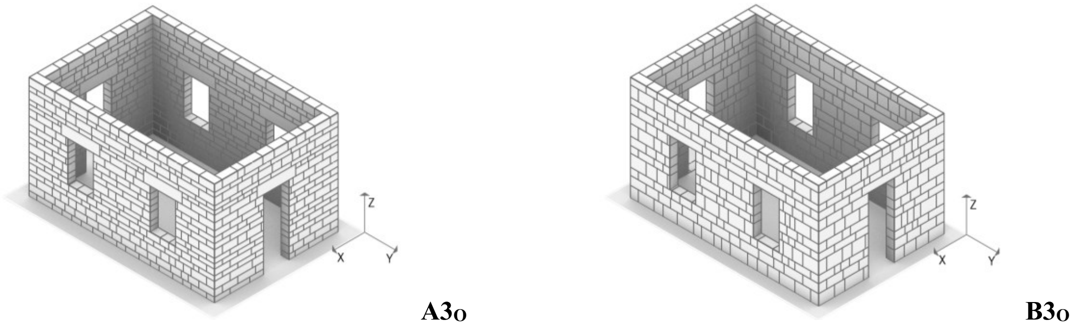

A3O B3O

Figure 10: Mesh discretisations adopted for the numerical investigations, with a total of ten.

As mentioned in section 2, DMEM approach requires defining the mechanical properties considering the failure modes, i.e., flexural, shear-diagonal and shear-sliding, independently. A nonlinearconstitutive law has been assumed for the flexural response, governed by an exponential softening for the tensile post-peak behaviour and a parabolic curve for the compressive post-peak behaviour. The shear-sliding behaviour has been considered according to a Mohr-Coulomb failure criterion, considering a perfectly post-elastic constitutive law and assuming that the cohesion under no confinement conditions is equal to the tensile strength. Regarding the shear-diagonal behaviour, a linear-elastic constitutive law has been adopted to avoid the shear failure of the element, i.e., a mesoscale approach [56] without accounting for the failure of the units (assumed infinitely resistant).

Table 3 and Table 4 summarise the mechanical properties adopted across the numerical simulation. One can note how tensile strength and fracture energy have been assumed to be very small to simulate dry-stacked masonry.

Table 3: Mechanical properties adopted for the box prototype: flexural behaviour

	Flexural behaviour					
	Density	Young's modulus	Compressive strength	Compressive fracture energy	Tensile strength	Tensile fracture energy
Model	[kg/m^3]	[MPa]	[MPa]	[N/mm]	[MPa]	[N/mm]
Mesoscale	1800	1500	3.80	3.00	0.001	0.0001

Table 4: Mechanical properties adopted for the box prototype: shear behaviour

	Diagonal cracking behaviour				Sliding behaviour	
	Shear modulus	Failure criterion	τ_0	μ_d	c	μ_s
Model	[MPa]		[MPa]		[MPa]	
Mesoscale	580	-	-	-	0.001	0.6

4.2 Nonlinear static analysis

Nonlinear static analyses have been performed applying an incremental lateral force, proportional to the mass of the structure, in X+ direction (Figure 8). Figure 8 also represents the control point used to define the pushover curves, which corresponds to the middle node at the top of the longitudinal wall that exhibits the maximum out of plane displacement.

Figure 11a and Figure 11b report the pushover curves for classes A and B characterised by a different number on the units' courses equal to 18 and 12, respectively. As stated above, for each class, five masonry patterns characterised by an increased index of randomness and the presence of openings have been generated (Figure 10). Results demonstrate how irregular masonry patterns, as well as the presence of the openings, tend to decrease the capacity of the structures.

As mentioned earlier, reference macro-element mesh discretisation has been compared with the random generated models (A2, A3, B2, B3) as well as with regular mesoscale configuration (A1, B1). To this end, reverse engineering was considered for selected mechanical parameters to get a good match in terms of structural response between macroscale and mesoscale models. In order to simulate the interlocking effect, in the macroscale model, the shear-diagonal behaviour has been calibrated according to a Turnsek-Cacovic failure criterion assuming a perfectly post-elastic law. The shear strength in the absence of axial load has been assumed to be equal 0.2 MPa while a value of 0.6 has been considered for the friction coefficient μ_s. The tensile strength f_t and the cohesion c, which affected the peak of the capacity curve, have been increased to 0.025 MPa in macro-model A and to 0.015 MPa in macro-model B with the aim to satisfactorily reproduce the static nonlinear response of the mesoscale models A1 and B1, respectively. Moreover, the value of tensile fracture energy G_{ft}, which influenced the post-peak capacity as reported in Ref. [49], was increased to 0.25 and 0.30 N/mm in the constitutive law of model A and B, respectively. It is worth noting that the interlocking phenomenon effect on the initial stiffness is less pronounced than the previously analysed U-shape. It happens because the interlocking phenomenon tends to increase the structure's initial stiffness, particularly when the slenderness ratio is small.

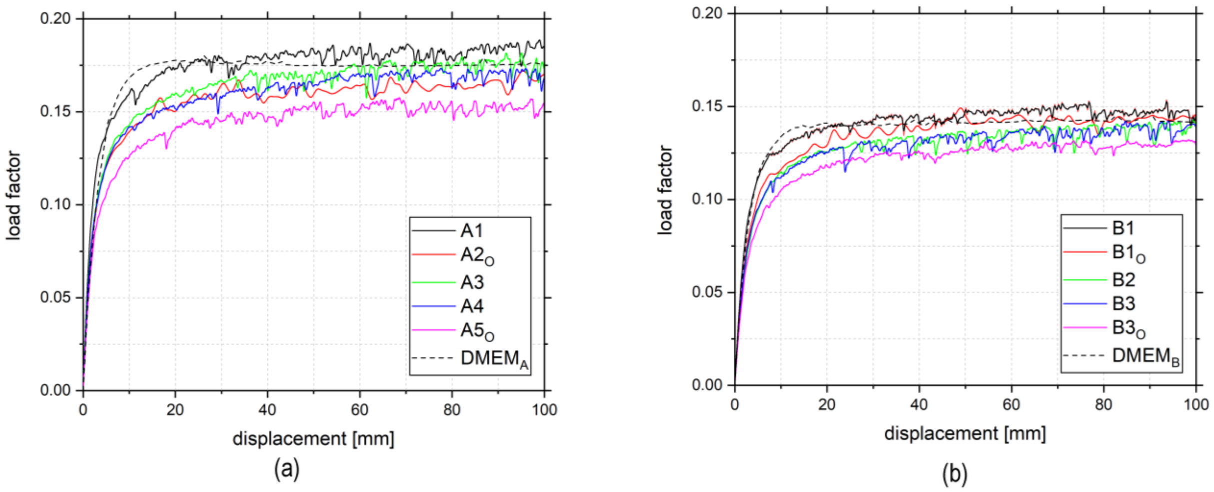

Figure 11: Comparison in terms of load-displacement curves for classes A and B characterised by a different number on the units' courses equal to: (a) 18; (b) 12.

Furthermore, the deformed shapes at the last step of the analyses, highlighting the collapse mechanisms of the structures and the concentration of plastic strains, are reported in Figure 12. The failure mechanisms are always characterised by the overturning of the wall orthogonally loaded and subjected to outwards actions. In this regard, it is observed how the plastic strains are mainly concentrated at the connection with the sidewalls. It is worth noting how increasing the randomness index, the collapse mechanism is more localised at a single wall, and the structure tends to rapidly lose the box behaviour, whereas, in the structure with a regular masonry pattern, the overall structural behaviour is affected by a more global character although the incipient collapse mechanism is still characterised by the collapse of the wall that tends to overturn OOP.

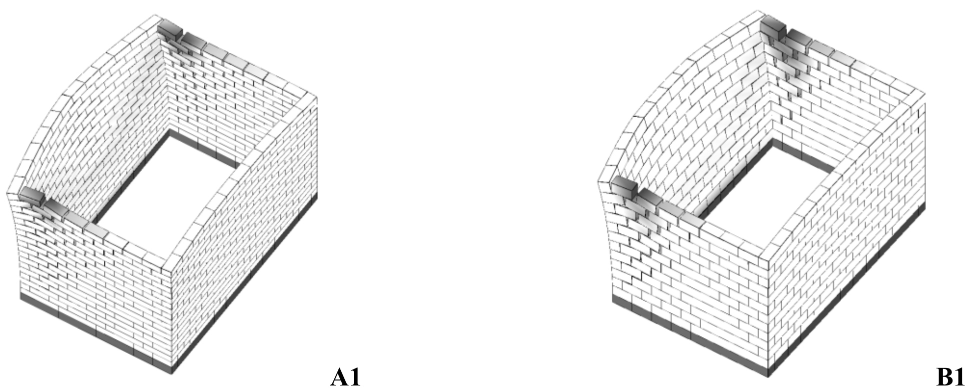

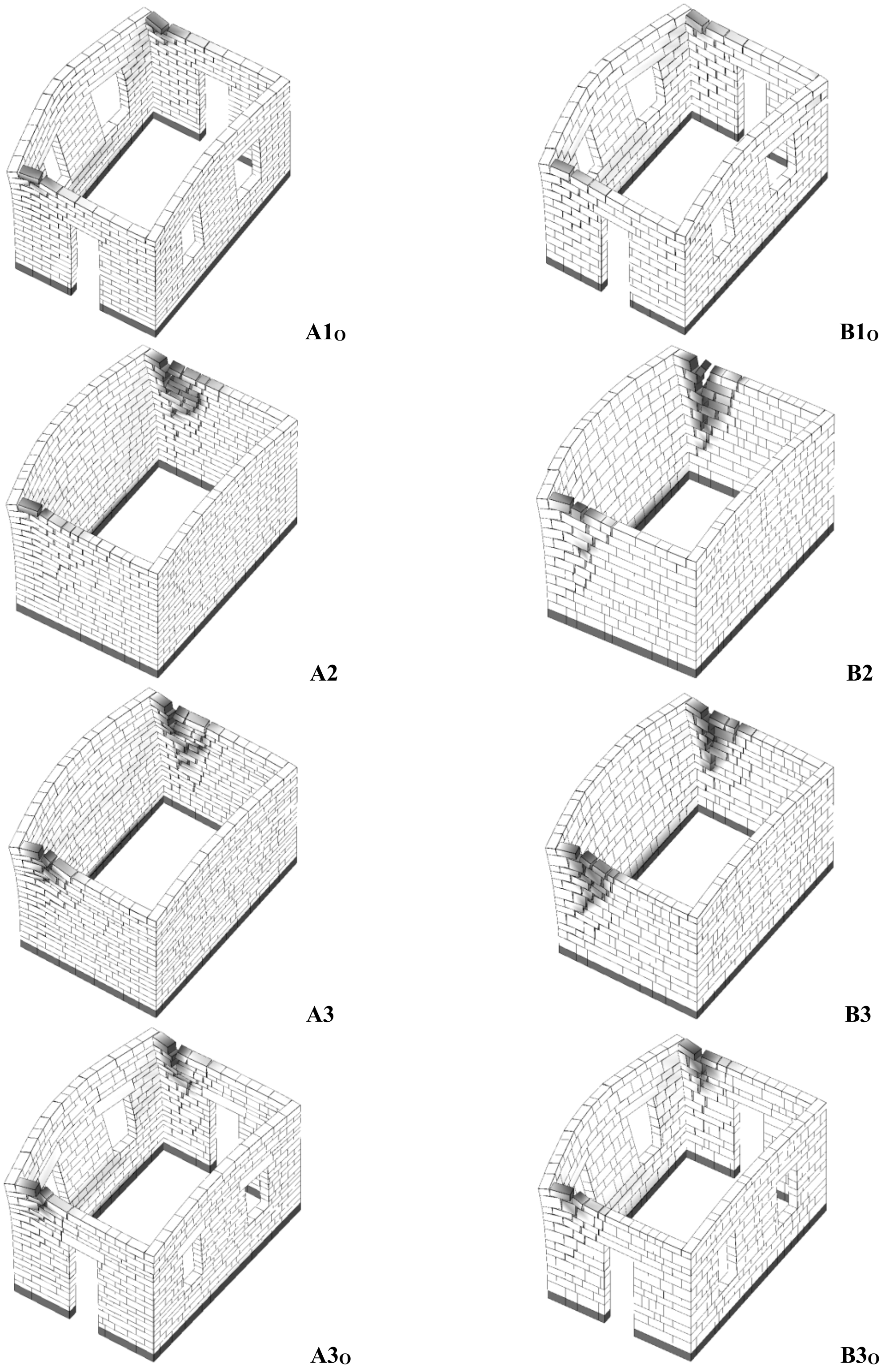

Figure 12: Deformed shapes of the mesh discretisations adopted for control point displacement equal to 100 mm.

For the sake of clarity, the histogram reported in Figure 13 represents the maximum displacement reached at the end of the simulations for the mesh configuration A1$_O$ and A3$_O$ evaluated by monitoring two control points located in the middle of the two opposite long walls. The same analysis has been reported regarding the configuration B1$_{O}$ and B3$_{O}$. In both cases, the results have been normalised with respect to the greater of the maximum displacements reached by the two points, and they quantitatively demonstrate how a chaotic distribution tends to localise the collapse mechanism leading to a negative influence on the masonry prototypes' global behaviour.

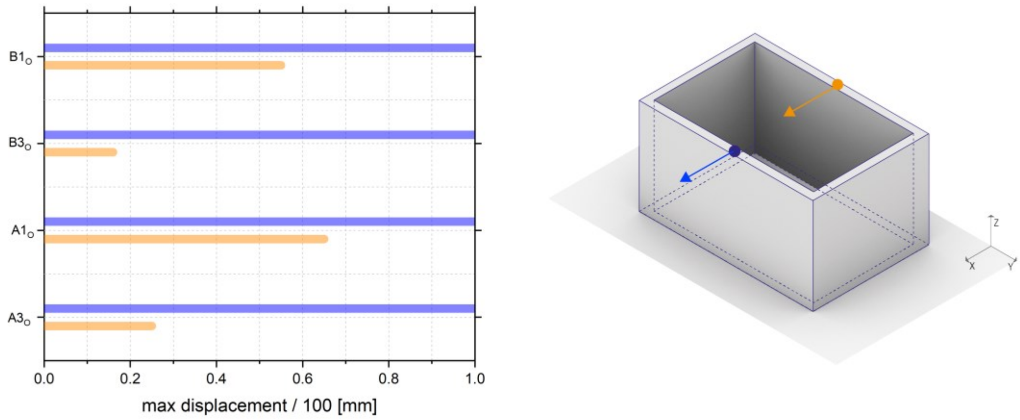

Figure 13: Comparisons in terms of maximum displacement reached: orange vs blue control point. Notation 1 indicates a regular masonry pattern and notation 3 indicates an irregular masonry pattern.

4.3 Nonlinear dynamic analysis

In this section, dynamic simulations have been performed applying a semi-sinusoidal pulse with an amplitude equal to 1g and a frequency of 6.7 Hz (that is a frequency close to the first mode vibration of the model A1) as input ground motion along the X direction (see Figure 14). Newmark's method with parameters $\gamma = 0.5$ and $\beta = 0.25$ [61], and a time step of 0.005 s has been adopted as numerical integration procedure, whereas the energy dissipation was based on the Rayleigh viscous damping criterion [62], assuming a 5% damping ratio associated with the 1st and 13th natural frequencies, the latter corresponding to 80% of the total accumulated specimen mass.

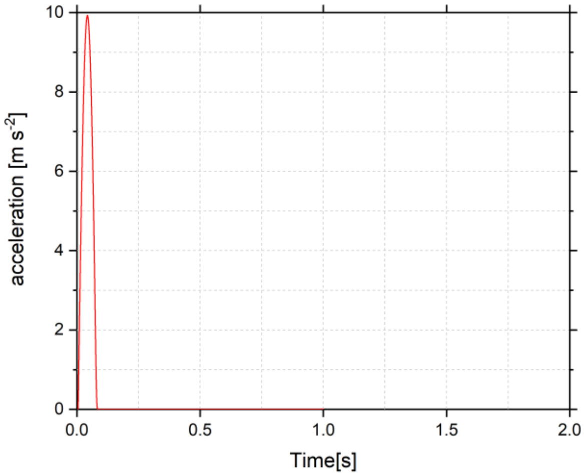

Figure 14: Ground motion input: semi-sinusoidal pulse.

Figure 15 a and b report the time-history displacement of the control point of the mesoscale patterns belonging to classes A and B. Similar to what is underlined within the nonlinear static analyses (with lower capacity in terms of forces), the mesh discretisations belonging to class B (low number of units' courses) show higher residual displacements. Indeed, B models are affected statistically by a smaller m parameter, i.e., the ratio between the half-length and height of the blocks, being class B characterised by fewer courses. It results in an overall lower capability of the blocks to generate frictional resistance in their plane [63].

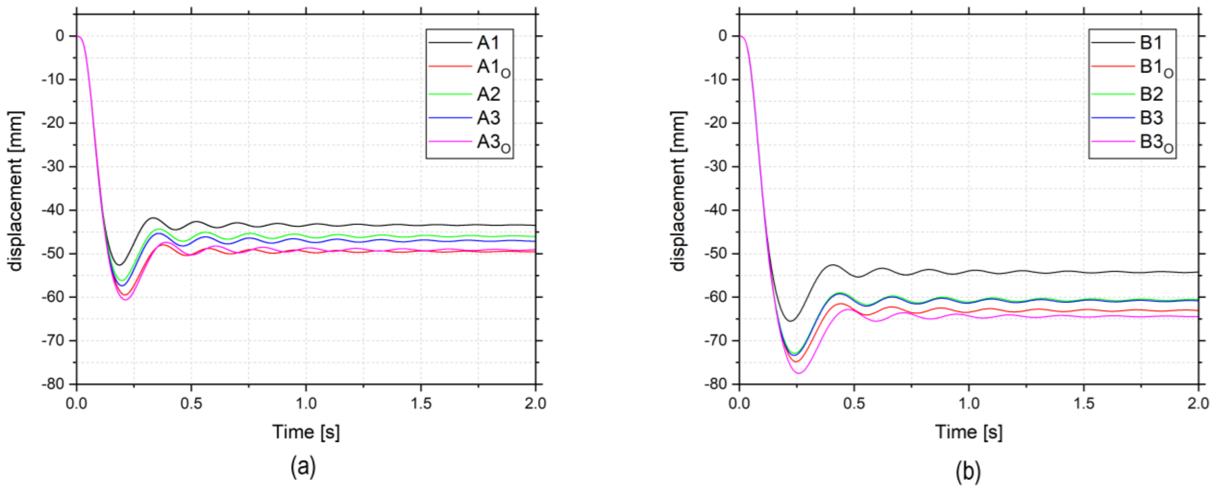

Figure 15: Comparison in terms of time history displacement.

Figure 15a and Figure 15b show how increasing the masonry pattern's randomness, the structures are affected by larger displacements. Similarly, larger displacements are found in cases with openings, for which the structures are obviously affected by lower global stiffness. Finally, aiming to investigate the dynamic response of the considered specimens when subjected to earthquake loading, incremental dynamic analysis (IDA) has been carried out by adopting the Amatrice EW (2016) earthquake record, Italy, as input ground motion active along the X-direction (see Figure 16a). The original record has been scaled in order to reach the condition of the near-collapse of the investigated masonry prototype.

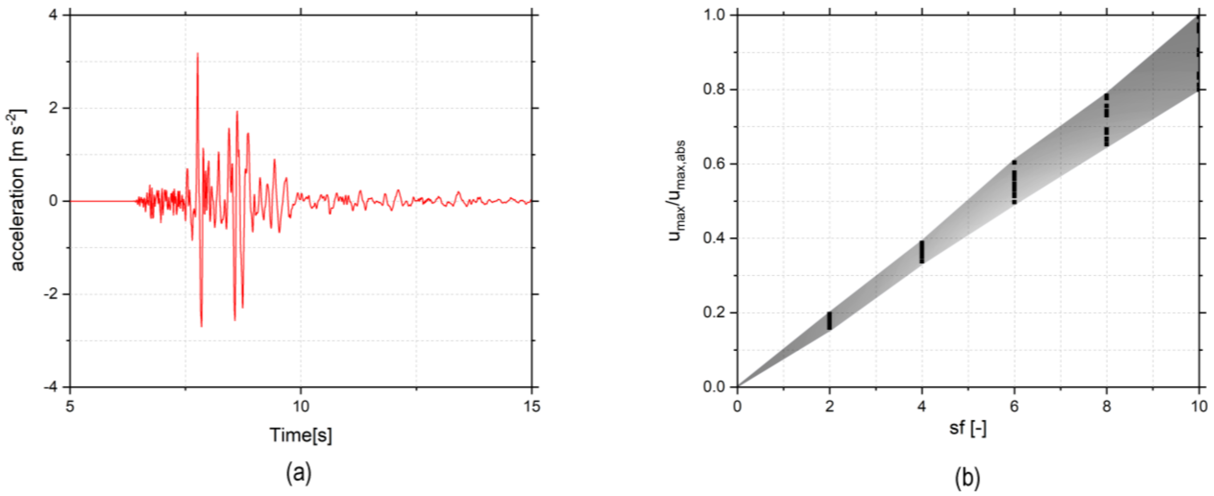

Figure 16: (a) Amatrice EW (2016) record; (b) ratio between the maximum displacement of the control point and the absolute maxi-mum displacement for all mesh discretisations as a function of the scale factor of the record: shaded red provides the envelope of the results.

Figure 16b reports the ratio between the maximum displacement of the control point and the absolute maximum displacement for all the investigated adopted mesh discretisations as a function of the scale factor of the record, which is a measure of the ground motion intensity (IM). It should be underlined that the adopted mesh configurations have shown a divergent behaviour with the increase of the scale factor, pointing out that the influence of the mesh pattern is larger, in terms of the maximum reached displacement, for a higher value of PGA. The results also confirm the need to perform stochastic simulations by generating a large number of masonry pattern configurations statistically consistent.

5 Final remarks

This paper investigates the DMEM approach by adopting a mesoscale representation rather than a classical macroscale representation. At first, parametric analyses investigate the mesh sensitivity of the DMEM approach and shed light on the mechanical parameters that need to be calibrated to consider physical phenomena, namely interlocking behaviour generated by the vertical joint misalignment. Such investigations were performed by using a benchmark model represented by a U-shape masonry prototype made in stone, idealising the experimental tests performed at the LNEC shaking table [55]. The results underlined the need to recalibrate the tensile fracture energy as well as the tensile strength. Furthermore, the comparisons with a classical FE homogeneous model calibrated in ABAQUS showed that DMEM requires much lower computational demand, also if the adopted discrete modelling approach contemplated a unit by unit mesoscale modelling.

In order to adequately simulate URM structures characterised by units with variable dimensions, a random masonry pattern generator was developed and implemented in a GHPython script. Such a script was adopted to generate 10 masonry prototypes (with different level of randomness), with the overall dimension consistent with a rectangular plan having 4.80 m and 7.20 m and walls' height equal to 4.0 m, in order to evaluate how the chaotic distribution of the units might affect the structural behaviour. Both nonlinear static and dynamic analyses were performed, and the results demonstrated how the masonry pattern affected the structural response. In particular, it was worth noting how the increase of the randomness degree generated an early loss of the box behaviour.

The main conclusions of this study are that:

1. DMEM approach is able to take into account the main in-plane and out-of-plane failure mechanisms;
2. Mesoscale configurations have been compared with a classical macro-element mesh discretisation. To this end, it was necessary to calibrate some mechanical parameters in order to get a good match in terms of structural response.
3. A digital tool was adopted to generate random masonry patterns; it can generate chaotic masonry patterns by defining a few parameters.

4. The results demonstrated how the arrangement of the blocks affected the results. Moreover, by increasing the randomness index, the collapse mechanism is localised, and the structures lose the box behaviour, whereas, in the structure with a regular masonry pattern, the overall structural behaviour exhibited a more global character.
5. Further investigations are necessary to better understand the potential of the DMEM approach in handling a mesoscale model and to have a clear picture of the influence of mesh discretisation on mechanical properties.
6. Further efforts are also required to implement a masonry pattern generator by taking into account geometrical parameters easily detectable from practitioners, i.e., masonry quality index [64].

Future studies could include: i) statistical definition of the mechanical properties [65], [66]; ii) simulation of strengthening techniques, such as the use of Textile Reinforced Matrix (TRM) of Fiber Reinforced Polymers (FRP) reinforcement, for masonry pattern having units of variable dimensions.

Author contribution statement:

Federica Vadalà: Conceptualisation, Methodology, Software, Writing—Original draft preparation, Validation. **Valeria Cusmano**: Conceptualisation, Methodology, Software, Visualisation, Writing—Original draft preparation, Validation, Writing—Original draft preparation. **Marco Francesco Funari**: Conceptualisation, Methodology, Software, Random mesh generator Visualisation, Supervision, Validation, Writing—Original draft preparation, Writing—Reviewing and Editing. **Ivo Caliò**: Software, Writing—Reviewing and Editing. **Paulo B. Lourenço**: Writing—Reviewing and Editing. All authors have read and agreed to the published version of the manuscript.

Funding:

This work was partly financed by FCT/MCTES through national funds (PIDDAC) under the R&D Unit Institute for Sustainability and Innovation in Structural Engineering (ISISE), under reference UIDB/04029/2020.

This work was partly funded by project STAND4HERITAGE that has received funding from the European Research Council (ERC) under the European Union's Horizon 2020 research and innovation programme (Grant agreement No. 833123), as an Advanced Grant.
This research was partially supported by the EWAS Project "an Early WArning System for Cultural Heritage" (ARS021_00926) PNR 2015-2020 Area di Specializzazione" CULTURAL HERITAGE". CUP E66C18000380005.

References

[1] M. Milić *et al.*, "Assessment and Rehabilitation of Culturally Protected Prince Rudolf Infantry Barracks in Zagreb after Major Earthquake," *Build 2021, Vol 11, Page 508*, vol. 11, no. 11, p. 508, Oct. 2021, doi: 10.3390/BUILDINGS11110508.

[2] L. Lulić, K. Ožić, T. Kišiček, I. Hafner, and M. Stepinac, "Post-Earthquake Damage Assessment—Case Study of the Educational Building after the Zagreb Earthquake," *Sustain 2021, Vol 13, Page 6353*, vol. 13, no. 11, p. 6353, Jun. 2021, doi: 10.3390/SU13116353.

[3] M. Diaferio, D. Foti, M. F. Sabbà, and M. Lerna, "A procedure for the seismic risk assessment of the cultural heritage," *Bull Earthq Eng*, vol. 19, no. 2, pp. 1027–1050, 2021.

[4] S. Silvestri *et al.*, "Shaking table testing of groin vaults made by 3D printers," *Soil Dyn Earthq Eng*, vol. 150, p. 106880, 2021.

[5] D. Foti and V. Vacca, "EXPERIMENTAL INVESTIGATION OF THE SEISMIC RESPONSE OF A MULTI-DRUM COLUMN," *WIT Trans Eng Sci*, vol. 118, pp. 11–19, 2017.

[6] S. Sharma, L. C. Silva, F. Graziotti, G. Magenes, and G. Milani, "Modelling the experimental seismic out-of-plane two-way bending response of unreinforced periodic masonry panels using a non-linear discrete homogenized strategy," *Eng Struct*, vol. 242, p. 112524, Sep. 2021, doi: 10.1016/J.ENGSTRUCT.2021.112524.

[7] J. A. Dauda, L. C. Silva, P. B. Lourenço, and O. Iuorio, "Out-of-plane loaded masonry walls retrofitted with oriented strand boards: Numerical analysis and influencing parameters," *Eng Struct*, vol. 243, p. 112683, 2021.

[8] G. Fortunato, M. F. Funari, and P. Lonetti, "Survey and seismic vulnerability assessment of the

Baptistery of San Giovanni in Tumba (Italy)," *J Cult Herit*, vol. 26, pp. 64–78, 2017, doi: 10.1016/j.culher.2017.01.010.

[9] D. Malomo, A. Mehrotra, and M. J. DeJong, "Distinct element modeling of the dynamic response of a rocking podium tested on a shake table," *Earthq Eng Struct Dyn*, vol. 50, no. 5, pp. 1469–1475, 2021.

[10] A. M. D'altri *et al.*, "Modeling Strategies for the Computational Analysis of Unreinforced Masonry Structures: Review and Classification," vol. 27, pp. 1153–1185, 2020, doi: 10.1007/s11831-019-09351-x.

[11] S. Karimzadeh, K. Kadas, A. Askan, M. A. Erberik, and A. Yakut, "Derivation of analytical fragility curves using SDOF models of masonry structures in Erzincan (Turkey)," *Earthquakes Struct*, vol. 18, no. 2, pp. 249–261, 2020.

[12] L. Cascini, R. Gagliardo, and F. Portioli, "LiABlock_3D: A Software Tool for Collapse Mechanism Analysis of Historic Masonry Structures," *Int J Archit Herit*, vol. 14, no. 1, pp. 75–94, 2020, doi: 10.1080/15583058.2018.1509155.

[13] G. De Felice and R. Giannini, "Out-of-plane seismic resistance of masonry walls," *J Earthq Eng*, vol. 5, no. 2, pp. 253–271, 2001, doi: 10.1080/13632460109350394.

[14] C. Casapulla, L. Cascini, F. Portioli, and R. Landolfo, "3D macro and micro-block models for limit analysis of out-of-plane loaded masonry walls with non-associative Coulomb friction," 2014, doi: 10.1007/s11012-014-9943-8.

[15] M. F. Funari, L. C. Silva, E. Mousavian, and P. B. Lourenço, "Real-time Structural Stability of Domes through Limit Analysis: Application to St. Peter's Dome," *https://doi.org/10.1080/15583058.2021.1992539*, pp. 1–23, Oct. 2021, doi: 10.1080/15583058.2021.1992539.

[16] A. Giuffré, "A Mechanical Model for Statics and Dynamics of Historical Masonry Buildings," in *Protection of the Architectural Heritage Against Earthquakes*, Springer Vienna, 1996, pp. 71–152.

[17] D. D'Ayala and E. Speranza, "Definition of Collapse Mechanisms and Seismic Vulnerability of Historic Masonry Buildings," *Earthq Spectra*, vol. 19, no. 3, pp. 479–509, 2003, doi:

10.1193/1.1599896.

[18] M. F. Funari, A. Mehrotra, and P. B. Lourenço, “A Tool for the Rapid Seismic Assessment of Historic Masonry Structures Based on Limit Analysis Optimisation and Rocking Dynamics,” *Appl Sci*, vol. 11, no. 3, p. 942, Jan. 2021, doi: 10.3390/app11030942.

[19] M. F. Funari, S. Spadea, P. Lonetti, F. Fabbrocino, and R. Luciano, “Visual programming for structural assessment of out-of-plane mechanisms in historic masonry structures,” *J Build Eng*, vol. 31, Sep. 2020, doi: 10.1016/j.jobe.2020.101425.

[20] M. F. Funari, S. Spadea, M. Ciantia, P. Lonetti, and F. Greco, “Visual programming for the structural assessment of historic masonry structures,” 2020.

[21] G. Fortunato, M. F. Funari, and P. Lonetti, “Survey and seismic vulnerability assessment of the Baptistery of San Giovanni in Tumba (Italy),” *J Cult Herit*, 2017, doi: 10.1016/j.culher.2017.01.010.

[22] L. C. Silva, N. Mendes, P. B. Lourenço, and J. Ingham, “Seismic Structural Assessment of the Christchurch Catholic Basilica, New Zealand,” *Structures*, vol. 15, pp. 115–130, Aug. 2018, doi: 10.1016/J.ISTRUC.2018.06.004.

[23] S. Szabó, A. Kövesdi, Z. Vasáros, Á. Csicsely, and D. Hegyi, “The cause of damage and failure of the Mud-brick vault of the Khan in New-Gourna,” *Eng Fail Anal*, vol. 128, p. 105567, Oct. 2021, doi: 10.1016/J.ENGFAILANAL.2021.105567.

[24] M. F. Funari, A. E. Hajjat, M. G. Masciotta, D. V. Oliveira, and P. B. Lourenço, “A Parametric Scan-to-FEM Framework for the Digital Twin Generation of Historic Masonry Structures,” *Sustain 2021, Vol 13, Page 11088*, vol. 13, no. 19, p. 11088, Oct. 2021, doi: 10.3390/SU131911088.

[25] M. Lerna, M. F. Sabbà, M. Diaferio, L. Carnimeo, S. Ivorra, and D. Foti, “Seismic risk assessment of a medieval tower: The case study of Craco,” 2020.

[26] N. Hoveidae, A. Fathi, and S. Karimzadeh, “Seismic damage assessment of a historic masonry building under simulated scenario earthquakes: A case study for Arge-Tabriz,” *Soil Dyn Earthq Eng*, vol. 147, p. 106732, 2021, doi: https://doi.org/10.1016/j.soildyn.2021.106732.

[27] P. Roca, M. Cervera, L. Pelà, R. Clemente, and M. Chiumenti, “Continuum FE models for the

analysis of Mallorca Cathedral," *Eng Struct*, vol. 46, pp. 653–670, Jan. 2013, doi: 10.1016/j.engstruct.2012.08.005.

[28] J. V. Lemos, "Discrete element modeling of masonry structures," *Int J Archit Herit*, vol. 1, no. 2, pp. 190–213, 2007, doi: 10.1080/15583050601176868.

[29] J. V. Lemos, "Discrete element modeling of the seismic behavior of masonry construction," *Buildings*, vol. 9, no. 2, 2019, doi: 10.3390/buildings9020043.

[30] T. T. Bui, A. Limam, V. Sarhosis, and M. Hjiaj, "Discrete element modelling of the in-plane and out-of-plane behaviour of dry-joint masonry wall constructions," *Eng Struct*, vol. 136, no. October, pp. 277–294, 2017, doi: 10.1016/j.engstruct.2017.01.020.

[31] S. Gonen, B. Pulatsu, E. Erdogmus, E. Karaesmen, and E. Karaesmen, "Quasi-static nonlinear seismic assessment of a fourth century A.D. Roman Aqueduct in Istanbul, Turkey," *Heritage*, vol. 4, no. 1, pp. 401–421, 2021, doi: 10.3390/heritage4010025.

[32] J. Kim, F. Lorenzoni, M. Salvalaggio, and M. R. Valluzzi, "Seismic vulnerability assessment of free-standing massive masonry columns by the 3D Discrete Element Method," *Eng Struct*, vol. 246, p. 113004, 2021, doi: https://doi.org/10.1016/j.engstruct.2021.113004.

[33] F. Clementi, V. Gazzani, M. Poiani, and S. Lenci, "Assessment of seismic behaviour of heritage masonry buildings using numerical modelling," *J Build Eng*, vol. 8, pp. 29–47, Dec. 2016, doi: 10.1016/j.jobe.2016.09.005.

[34] S. Chen, A. Ferrante, F. Clementi, and K. Bagi, "DEM analysis of the effect of bond pattern on the load bearing capacity of barrel vaults under vertical loads," *Int J Mason Res Innov*, vol. 6, no. 3, pp. 346–373, 2021.

[35] D. Foti, V. Vacca, and I. Facchini, "DEM modeling and experimental analysis of the static behavior of a dry-joints masonry cross vaults," *Constr Build Mater*, vol. 170, pp. 111–120, 2018.

[36] N. Savalle, É. Vincens, and S. Hans, "Experimental and numerical studies on scaled-down dry-joint retaining walls: Pseudo-static approach to quantify the resistance of a dry-joint brick retaining wall," *Bull Earthq Eng*, vol. 18, no. 2, pp. 581–606, 2020.

[37] V. Sarhosis, J. V Lemos, and K. Bagi, "Chapter 13 - Discrete element modeling," in *Woodhead Publishing Series in Civil and Structural Engineering*, B. Ghiassi and G. B. T.-N. M. of M. and

H. S. Milani, Eds. Woodhead Publishing, 2019, pp. 469–501.

[38] P. B. Lourenço and L. C. Silva, "Computational applications in masonry structures: From the meso-scale to the super-large/super-complex," *Int J Multiscale Comput Eng*, vol. 18, no. 1, pp. 1–30, 2020, doi: 10.1615/IntJMultCompEng.2020030889.

[39] M. F. Funari, L. C. Silva, N. Savalle, and P. B. Lourenço, "A concurrent micro/macro FE-model optimized with a limit analysis tool for the assessment of dry-joint masonry structures," *Int J Multiscale Comput Eng*, vol. In Press, 2022, doi: 10.1615/IntJMultCompEng.2021040212.

[40] D. Malomo and M. J. DeJong, "A Macro-Distinct Element Model (M-DEM) for simulating the in-plane cyclic behavior of URM structures," *Eng Struct*, vol. 227, no. April 2020, p. 111428, 2021, doi: 10.1016/j.engstruct.2020.111428.

[41] A. M. D'Altri, N. Lo Presti, N. Grillanda, G. Castellazzi, S. de Miranda, and G. Milani, "A two-step automated procedure based on adaptive limit and pushover analyses for the seismic assessment of masonry structures," *Comput Struct*, vol. 252, p. 106561, Aug. 2021, doi: 10.1016/j.compstruc.2021.106561.

[42] D. Malomo and M. J. DeJong, "A Macro-Distinct Element Model (M-DEM) for out-of-plane analysis of unreinforced masonry structures," *Eng Struct*, vol. 244, no. April, p. 112754, 2021, doi: 10.1016/j.engstruct.2021.112754.

[43] E. Quagliarini, G. Maracchini, and F. Clementi, "Uses and limits of the Equivalent Frame Model on existing unreinforced masonry buildings for assessing their seismic risk: A review," *J Build Eng*, vol. 10, pp. 166–182, Mar. 2017, doi: 10.1016/J.JOBE.2017.03.004.

[44] R. Siano *et al.*, "Numerical investigation of non-linear equivalent-frame models for regular masonry walls," *Eng Struct*, vol. 173, pp. 512–529, 2018, doi: https://doi.org/10.1016/j.engstruct.2018.07.006.

[45] I. Caliò, M. Marletta, and B. Pantò, "A new discrete element model for the evaluation of the seismic behaviour of unreinforced masonry buildings," *Eng Struct*, vol. 40, pp. 327–338, 2012, doi: 10.1016/j.engstruct.2012.02.039.

[46] B. Pantò, F. Cannizzaro, I. Caliò, and P. B. Lourenço, "Numerical and Experimental Validation of a 3D Macro-Model for the In-Plane and Out-Of-Plane Behavior of Unreinforced Masonry

Walls," *Int J Archit Herit*, vol. 11, no. 7, pp. 946–964, 2017, doi: 10.1080/15583058.2017.1325539.

[47] F. Cannizzaro, B. Pantò, S. Caddemi, and I. Caliò, "A Discrete Macro-Element Method (DMEM) for the nonlinear structural assessment of masonry arches," *Eng Struct*, vol. 168, no. October 2020, pp. 243–256, 2018, doi: 10.1016/j.engstruct.2018.04.006.

[48] C. Chácara, P. B. Lourenço, B. Pantò, F. Cannizzaro, and I. Caliò, "Macro-element mass matrix for the dynamic assessment of unreinforced masonry structures," 2017.

[49] B. Pantò, L. Silva, G. Vasconcelos, and P. B. Lourenço, "Macro-modelling approach for assessment of out-of-plane behavior of brick masonry infill walls," *Eng Struct*, vol. 181, no. November 2018, pp. 529–549, 2019, doi: 10.1016/j.engstruct.2018.12.019.

[50] C. Chácara, F. Cannizzaro, B. Pantò, I. Caliò, and P. B. Lourenço, "Seismic vulnerability of URM structures based on a Discrete Macro-Element Modeling (DMEM) approach," *Eng Struct*, vol. 201, p. 109715, Dec. 2019, doi: 10.1016/j.engstruct.2019.109715.

[51] F. Cannizzaro, "The seismic behavior of historical buildings: a macro-element approach," University of Catania, 2010.

[52] V. Turnšek and F. Čačovič, "Some experimental results on the strength of brick masonry walls," *Proc 2nd Int Brick Mason Conf*, pp. 149–156, 1971.

[53] I. Caliò and B. Pantò, "A macro-element modelling approach of Infilled Frame Structures," *Comput Struct*, vol. 143, pp. 91–107, 2014, doi: 10.1016/j.compstruc.2014.07.008.

[54] F. Peña, "A Semi-Discrete Approach for the Numerical Simulation of Freestanding Blocks," no. June, pp. 416–439, 2016, doi: 10.4018/978-1-5225-0231-9.ch016.

[55] P. X. Candeias, A. Campos Costa, N. Mendes, A. A. Costa, and P. B. Lourenço, "Experimental assessment of the out-of-plane performance of masonry buildings through shaking table tests," *Int J Archit Herit*, vol. 11, no. 1, pp. 31–58, 2017.

[56] F. Cannizzaro and P. B. Lourenço, "Simulation of Shake Table Tests on Out-of-Plane Masonry Buildings. Part (VI): Discrete Element Approach," *https://doi.org/10.1080/15583058.2016.1238973*, vol. 11, no. 1, pp. 125–142, Jan. 2016, doi: 10.1080/15583058.2016.1238973.

[57] V. Abaqus, "6.14 Documentation," *Dassault Syst Simulia Corp*, vol. 651, no. 6.2, 2014.

[58] S. Cattari *et al.*, "Nonlinear modeling of the seismic response of masonry structures: critical review and open issues towards engineering practice," *Bull Earthq Eng*, 2021.

[59] G. Milani and P. B. Lourenço, "A simplified homogenized limit analysis model for randomly assembled blocks out-of-plane loaded," *Comput Struct*, vol. 88, no. 11, pp. 690–717, 2010, doi: https://doi.org/10.1016/j.compstruc.2010.02.009.

[60] "The Python Language Reference — Python 3.9.5 documentation," 2021. https://docs.python.org/3/reference/ (accessed Jun. 15, 2021).

[61] N. M. Newmark, "A Method of Computation for Structural Dynamics," *J Eng Mech Div*, vol. 85, no. 3, pp. 67–94, Jul. 1959, doi: 10.1061/JMCEA3.0000098.

[62] A. Alipour and F. Zareian, "Study rayleigh damping in structures; uncertainties and treatments," in *the 14th world conference on earthquake engineering*, 2008, pp. 12–17.

[63] C. Casapulla and L. U. Argiento, "In-plane frictional resistances in dry block masonry walls and rocking-sliding failure modes revisited and experimentally validated," *Compos Part B Eng*, vol. 132, pp. 197–213, Jan. 2018, doi: 10.1016/J.COMPOSITESB.2017.09.013.

[64] A. Borri and A. De Maria, "L'indice di Qualità Muraria (IQM): Evoluzione ed Applicazione nell'Ambito delle Norme Tecniche per le Costruzioni del 2008," 2009.

[65] B. Pulatsu, S. Gonen, E. Erdogmus, P. B. Lourenço, J. V. Lemos, and R. Prakash, "In-plane structural performance of dry-joint stone masonry Walls: A spatial and non-spatial stochastic discontinuum analysis," *Eng Struct*, vol. 242, p. 112620, Sep. 2021, doi: 10.1016/J.ENGSTRUCT.2021.112620.

[66] B. Pulatsu, S. Gonen, E. Erdogmus, P. B. Lourenço, J. V. Lemos, and J. Hazzard, "Tensile Fracture Mechanism of Masonry Wallettes Parallel to Bed Joints: A Stochastic Discontinuum Analysis," *Model 2020, Vol 1, Pages 78-93*, vol. 1, no. 2, pp. 78–93, Oct. 2020, doi: 10.3390/MODELLING1020006.